International Journal of Heat and Mass Transfer 212 (2023) 124222

Contents lists available at ScienceDirect

International Journal of Heat and Mass Transfer

journal homepage: www.elsevier.com/locate/hmt

On/off switchable interfacial thermal resistance in graphene/fullerene/graphene heterostructures

Yixuan Xue[a], Harold S. Park[b], Jin-Wu Jiang[a,c,*]

[a] Shanghai Key Laboratory of Mechanics in Energy Engineering, Shanghai Institute of Applied Mathematics and Mechanics, School of Mechanics and Engineering Science, Shanghai University, Shanghai 200072, People's Republic of China
[b] Department of Mechanical Engineering, Boston University, Boston, Massachusetts 02215, USA
[c] Zhejiang Laboratory, Hangzhou 311100, China

ARTICLE INFO

Article history:
Received 15 December 2022
Revised 6 April 2023
Accepted 19 April 2023
Available online 15 May 2023

Keywords:
Graphene/fullerenes/graphene sandwiches
The kapitza resistance
Thermal hysteresis
Molecular dynamics simulation

ABSTRACT

Switchable thermal devices are attracting significant research interest as a basic thermal management component. In this work, taking graphene/fullerene/graphene sandwiches as an example, we demonstrate that the interfacial thermal resistance can show a switchable, step-like change by varying the number of fullerenes in the sandwich structure. Changing the number of fullerenes causes a structural transition between the graphene layers from adhered to separated, resulting in an enhancement of about a factor of two in the interfacial thermal resistance during this on/off switchable phenomenon, which we analyze using analytic expressions based on the thermal transport theory. We further illustrate that the switchable phenomenon can also be realized by applying mechanical strain or by varying the temperature of the sandwich structure. This work demonstrates that the sandwich-liked nanoscale heterostructures can exhibit hysteretic changes in heat transport, and thus have promise for potential applications in switchable thermal devices.

1. Introduction

Switchable thermal devices, which are similar to the electronic components of integrated circuits, have great potential for applications in thermal switches [1], thermal diodes [2], and logic elements [3]. These switchable thermal components allow the heat flux to switch between a heat-conducting 'on-state' and a heat-blocking 'off-state'. In the recent review article [4], many physical mechanisms and technologies were introduced to realize the thermal switch effect, including phase transition [5,6], chemical composition modification [7], cryogenically applied magnetic or electric fields [8,9], and so on.

Besides, the thermal switches can be realized by changing the bond strength and the microstructure at the interface region, which can effectively affect the thermal property. For example, Yu et al. found that the mixture of graphene and aluminum ions can form more compact packing structures and enhance the thermal conductivity by one order of magnitude [10]. Yang et al. found that the thermal conductivity of boron nanoribbon bundles can be switched by using different liquids to change the bonding strength between nanoribbons [11]. Yuzvinsky et al. designed a multi-layer carbon tube structure, where the phenomenon of thermal switching was realized by sliding the outer shells in a telescoping-like manner [12]. However, most of the designed interface structures need to be changed artificially to achieve a thermal switching phenomenon, which makes it difficult to be used in some extreme environments, such as nuclear radiation.

Novel structures, such as the sandwich-like heterostructure, may have significant potential to efficiently manipulate the thermal transport, which is important for thermal switches. The sandwich-like heterostructure can be constructed by stacking atomic layers in a layer-by-layer mode [13]. Not only can it adjust the thermal conductivity by changing the weight fraction of the interlayer [14], but also the structure is very sensitive to the environmental changes, such as temperature, resulting in different thermal conductivity [14,15]. For example, the degree of crystallinity of the epoxy resin is low at low temperature, and the thermal conductivity of Te/MoS_2/Ag-epoxy heterostructure at 5 wt% rises with the increase of temperature until the transition temperature is reached [15]. Different from other methods based on a single control technology, the thermal properties of sandwich-like heterostructure can also be effectively controlled by mechanical methods, because this van der Waals structure can be changed by strain. Thus, by changing experimental conditions or natural environments, the structure of sandwich-like heterostructures can be

* Corresponding author.
E-mail address: jwjiang5918@hotmail.com (J.-W. Jiang).

https://doi.org/10.1016/j.ijheatmasstransfer.2023.124222
0017-9310/

effectively controlled, thereby changing the thermal conductivity. It is quite interesting and critical to examine how the structural transitions of sandwich-like heterostructure will affect the thermal hysteresis in different environments.

As a special sandwich structure, the graphene/fullerene/graphene (GFG) sandwich, which has recently been observed experimentally, is a novel platform for multifunctional applications [16]. The GFG sandwich has already shown many superior and tunable physical properties, such as high thermoelectric figure of merit [17] and tunable wrinkle network [18]. Similarly, the GFG sandwich has plenty of novel configurations as a direct result of the extreme flexibility of graphene and the unique spherical structure of fullerenes [19]. For example, a small number of fullerenes can be enclosed by two graphene layers, i.e., these two outer graphene layers are adhered together. With the increase of the fullerene number, the outer two graphene layers will be separated, resulting in a structural transition.

Therefore, taking the GFG sandwich as an example, the interfacial thermal resistance (ITR) is systematically investigated by the heat dissipation method with molecular dynamics (MD) simulations in this work. We find a step-like jump in the ITR by varying the fullerene number, due to the structural transition for the graphene layers from an adhered configuration into a separated atomic configuration. The on/off switchable behavior is described by the analytic expressions derived based on the thermal transport theory. We further illustrate that the switchable phenomenon can be realized by applying mechanical strain or varying the temperature of the sandwich-like structure. These sandwich-like structures can thus lead to hysteretic changes in heat transport, which opens up new pathways for developing switchable thermal devices.

2. Structure and simulation details

As shown in Fig. 1, the GFG sandwiched structure includes three layers, where a fullerene layer is sandwiched by two graphene layers. The area of the square graphene layer is $A_0 = L^2$. The area ratio between the graphene and fullerene layers is defined as $\alpha = \frac{A}{A_0}$, where A is the area of the fullerene layer. The dimensions of GFG sandwiches in x and y directions are properly chosen so that the mismatch strain is less than 1%.

All MD simulations were performed by using the large-scale atomic/molecular massively parallel simulator (LAMMPS) package [20], while the VMD package is used for visualization [21]. Periodic boundary conditions were applied along the in-plane x and y directions to remove the edge effect, while free boundary conditions were applied in the out-of-plane direction. The adaptive intermolecular reactive empirical bond-order (AIREBO) potential was adopted to describe the covalent and van der Waals (vdW) interactions among carbon atoms, which has been successfully applied to investigate mechanical and thermal properties for graphene [22,23]. The Lennard-Jones (LJ) cutoff among all carbon atoms for the AIREBO potential is set to be 12 Å. The standard Newton equations of motion are integrated in time using the velocity Verlet algorithm [24] with a time step of 1 fs.

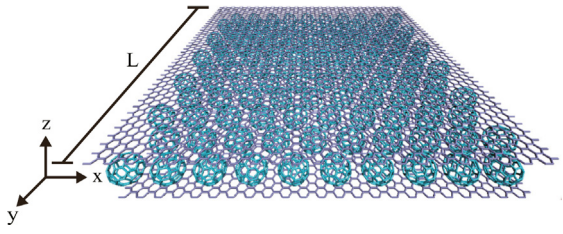

Fig. 1. Atomic structure for GFG sandwiches.

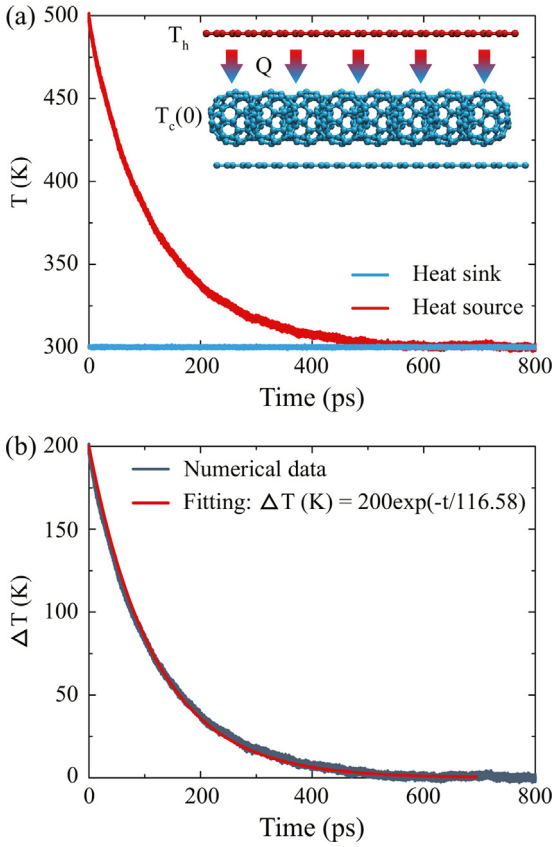

Fig. 2. The temperature difference during the heat dissipation process. (a) The time dependence for the temperature of the heat source and heat sink. The inset shows a schematic diagram of the heat dissipation model. (b) The evolution of the temperature difference during the heat dissipation process.

The thermal transport process is simulated using the heat dissipation method in this work [25], which mimics the experimental pump-probe approach as shown in Fig. 2(a). This method is widely used in the study of interfacial thermal transport [26,27]. There are three steps in the simulation. First, the relaxed configuration is equilibrated at a constant temperature and pressure within the isothermal-isobaric (NPT) ensemble for 0.6 ns. Second, an initial temperature difference is set up between the upper graphene layer and the lower graphene layer, by maintaining the constant temperature for these two parts with the Berendsen method [28], which has been frequently used to control the temperature in the research of thermal properties [27,29]. The main results are unchanged if the Langevin thermostat is used instead. The NVE (constant atom number, constant volume, and constant energy) ensemble is used in the second step. In the final step, the system is allowed to evolve freely within the NVE ensemble. The heat energy flows from the upper graphene layer into the lower part, so the temperature for the upper graphene layer (T_h) will decrease gradually. In the meantime, the temperature for the lower part ($T_c(0)$) is kept unchanged. The system reaches the equilibrium state when the entire system has the same temperature.

According to the Fourier's law and the definition of the heat capacity, the time dependence for the temperature T_h is governed by the following equation [25]:

$$C_v \rho d \frac{\partial T_h}{\partial t} = -\frac{1}{R_K}[T_h - T_c(0)], \quad (1)$$

where C_v, ρ, and d are the specific heat capacity, the mass density, and the thickness of graphene, respectively and R_K is the interfacial thermal resistance. From Eq. (1), the temperature difference,

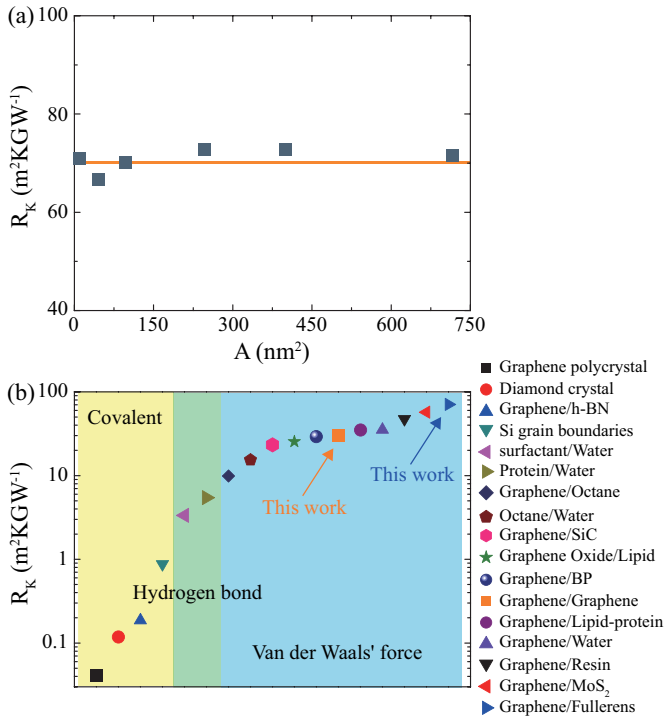

Fig. 3. The size effect on the ITR. (a) The ITR for the GFG structure with different dimensions. The horizontal line is a guide to the eyes. (b) A summary of the ITR of the interface constructed by the covalent bond (the yellow region), the hydrogen bond (the green region) and the van der Waals force (the blue region). The data are collected from the literature [27,29,31–43]. (For interpretation of the references to colour in this figure legend, the reader is referred to the web version of this article.)

$\Delta T(t) = T_h(t) - T_c(0)$, can be obtained as

$$\Delta T(t) = \Delta T_0 \exp(-t/\tau), \tag{2}$$

where $\Delta T_0 = T_h(0) - T_c(0)$ is the initial temperature difference. It has been shown that the initial temperature difference ΔT_0 has no effect on the ITR above 50 K [30], so we choose a proper value of $\Delta T_0 = 200$ K in the following calculations, which has also been used in some previous studies [26,27]. As shown in Fig. 2(b), the temperature difference can be well fitted to the theoretical result in Eq. (2), yielding the value of the thermal relaxation time $\tau = \frac{R_K C_v}{A}$. Then the interfacial thermal resistance can be calculated by [25]:

$$R_K = \frac{\tau A}{C_v}. \tag{3}$$

3. Results and discussion

3.1. Structure transition effect

We first examine the size effect on the ITR of the graphene/fullerene interface at room temperature. The fullerene layer is sandwiched by two graphene layers with the dimension from 2.94×3.39 nm^2 to 26.88×26.67 nm^2. As shown in Fig. 3(a), the ITR is about 69.19 m^2K/GW and is not sensitive to the area of the graphene/fullerene interface. This area insensitivity for the ITR has also been observed in the graphene/graphene [35] and graphene/black phosphorus [27] interfaces. The ITR of the graphene/fullerene interface is compared with the ITR value reported for some other interfaces in Fig. 3(b). The interface is divided into three categories according to the nature of the interfacial bonding properties, including the covalent bond (the yellow region), the hydrogen bonds (the green region) and the van der Waals force (the blue region). It can be seen that the ITR of the graphene/fullerene interface is the maximum value in the Fig. 3(b), which is about twice the ITR for the graphene/graphene interface.

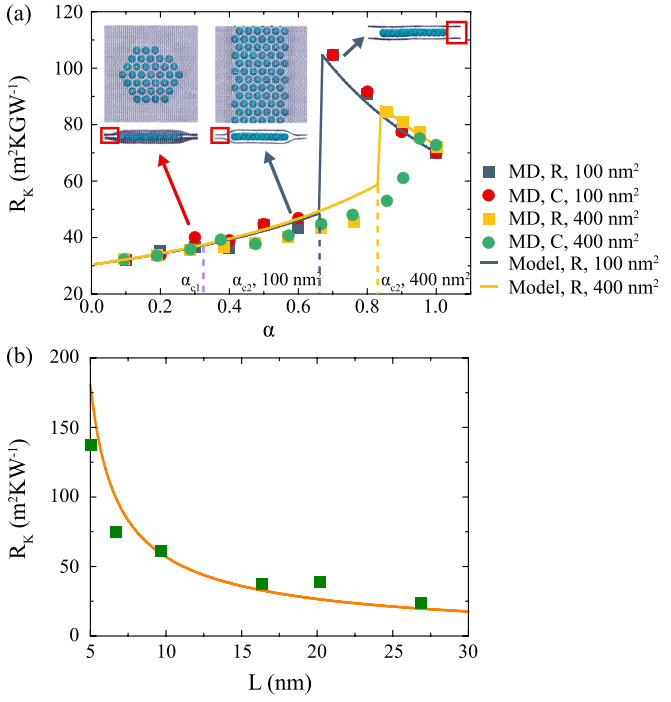

Fig. 4. The effect of the area ratio α on the ITR. (a) The dependence of the ITR on the area ratio α. Insets display the structural pattern for the GFG heterostructure. (b) The size dependence for the ITR jump at the critical point α_{c2}.

Before demonstrating the strong effect that the atomic configuration has on the ITR of the graphene/fullerene interface, we first demonstrate the structural transitions that can occur for this structure. In a recent work, we have disclosed that the structure of the GFG heterostructure is sensitive to the area ratio $\alpha = A_F/A_G$, where A_F and A_G are the areas of the fullerene and the graphene layers, respectively [19]. From the energy point of view, the configuration of the GFG sandwich structure is determined by two typical energies, i.e., the cohesive energy and the bending energy. There are two structure transitions that occur with increasing area ratio α. For a given number of fullerenes (with a specific value of α), the fullerene layer can be either in the circular pattern or the rectangular pattern. By comparing the stability of the two patterns, the most stable pattern can be obtained. For a given graphene bilayer, the most stable pattern of the fullerene layer will evolve from circular to rectangular at a critical ratio $\alpha_{c1} = 1/\pi$ with increasing fullerene number, as shown in the insets of Fig. 4(a). Note that the top and bottom graphene layers are adhered in both the circular and rectangular patterns. With further increasing fullerene number in the rectangular pattern, the cohesive energy between the graphene layers is reduced. Due to the competition between bending and cohesive energies, the GFG system transits from the adhered configuration into the separated configuration as displayed by the insets of Fig. 4(a). The critical value α_{c2} is described by the following analytic expression,

$$\alpha_{c2} = \frac{2\rho_b}{|g_c|L} - \frac{2c}{L}, \tag{4}$$

where $g_c = -0.019$ eV/Å is the cohesive energy density per area, $\rho_b = 0.075$ eV/Å is the bending energy density per length, c is a fitting parameter and L is the lateral dimension of the system. The GFG of two different dimensions are simulated. The critical value for the area ratio α_{c2} is size-dependent, and is 0.66 and 0.83 for

the structure of 9.94×9.60 nm^2 and 20.16×19.88 nm^2 structures, respectively.

We next study the effects of these two structure transitions on the ITR of the GFG system. There are several major features in Fig. 4(a). First, the ITR of GFG sandwiches rises gradually for $\alpha < \alpha_{c2}$. However, there is a sharp jump for the ITR at α_{c2}. This implies that the conduction across the GFG heterostructure is switchable in a wide range. Furthermore, the magnitude of the jump at α_{c2} depends on the size of the GFG heterostructure. The ITR decreases gradually with further increasing α for $\alpha > \alpha_{c2}$.

The gradual increase of the ITR with increasing area ratio α for $\alpha < \alpha_{c2}$ can be understood in terms of the interface adhesive strength. The adhesive strength between the spherical fullerenes and the flat graphene layer is weaker than the adhesive strength between two graphene layers because the contact area between the fullerene and graphene is smaller, due to the spherical shape of the fullerene. With the increase of the area ratio α, the graphene/graphene interfacial area is replaced by the graphene/fullerene interfacial area, so the overall adhesive strength of the interface is reduced and the ITR increases as a consequence. The ITR of the GFG sandwich structure can be calculated based on the interfacial thermal conductivity (ITC) of the graphene/graphene and graphene/fullerene interfaces:

$$\kappa = \alpha\kappa_0 + (1-\alpha)\kappa_1, \tag{5}$$

where $\kappa_0 = 0.014$ GW/m^{2}K is the ITC of the graphene/fullerene interface, and $\kappa_1 = 0.033$ GW/m^{2}K is the ITC of the graphene/graphene interface. The corresponding ITR is

$$R_k = \frac{1}{\kappa} = \frac{1}{\alpha\kappa_0 + (1-\alpha)\kappa_1}. \tag{6}$$

Fig. 4(a) shows that the analytic result in Eq. (6) is in good agreement with the MD simulation results for the GFG of different sizes.

The ITR shows a sharp jump at the second critical point α_{c2}. This ITR is enhanced by more than a factor of two as a result of this sharp jump. This jump in ITR is directly related to the structure transition from the adhered configuration into the separated configuration at the second critical point α_{c2}. As a result of the separation of the graphene layers, the heat conduction ability is significantly reduced for the GFG heterostructure, as the separated graphene segments do not contribute to the heat conduction. Thus, for the GFG with $\alpha > \alpha_{c2}$, the heat conduction is primarily due to the graphene/fullerene interface. The relationship between ITR and α is reduced to

$$R_k = \frac{1}{\alpha\kappa_0}. \tag{7}$$

Fig. 4(a) shows that the analytic result in Eq. (7) also qualitatively agrees with the MD results. In particular, this analytic expression is able to describe the MD result for the GFG of different sizes.

We now discuss the jump of the ITR at α_{c2} in Fig. 4(a). This jump phenomenon can be considered as an on/off switchable cross-plane thermal conductivity, which enables the GFG heterostructure to be potentially useful for switchable thermal components. Fig. 4(a) illustrates that the magnitude of the jump (ΔR_K) at α_{c2} depends on the size of the GFG heterostructure. For example, ΔR_K is 61.04 m^{2}K/GW and 38.65 m^{2}K/GW for the GFG of size 100 nm^2 and 400 nm^2, respectively. An analytic expression can be achieved for the size dependence of the jump magnitude by combining Eqs. (4), (6) and (7)

$$\Delta R_k = \frac{1}{\alpha_{c2}\kappa_0} - \frac{1}{\alpha_{c2}\kappa_0 + (1-\alpha_{c2})\kappa_1}. \tag{8}$$

Fig. 4(b) shows that the theoretical prediction by Eq. (8) is consistent with the simulation results. This downward trend of ITR shows that GFG sandwich structure has greater advantages for switchable thermal elements when the size is less than 20 nm.

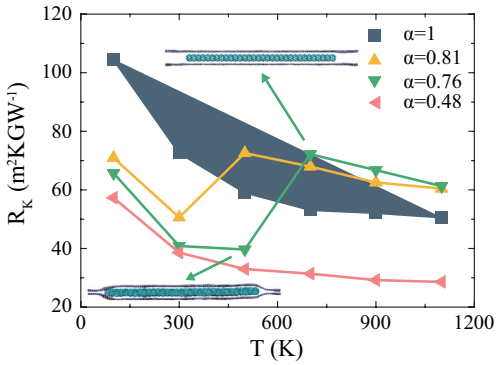

Fig. 5. The temperature dependence for the ITR. Insets display the atomic configuration for the GFG interface at 500 K and 700 K for the GFG structure with $\alpha = 0.76$.

3.2. Temperature effect

Thermal conductivity is known to be temperature-sensitive, and so we study the temperature effect on the ITR. We begin with a GFG heterostructure containing fullerenes in the rectangular pattern, with size 20.16×19.88 nm^2. We simulate the GFG sandwich structures with the area ratio α of 1.0, 0.81, 0.76 and 0.48. For $\alpha = 1.0$ (greater than α_2) and $\alpha = 0.48$ (less than α_2), there is no structure transition for the GFG sandwich with increasing temperature. Accordingly, the ITR decreases monotonically with the increase of temperature as shown in Fig. 5. Because the anharmonicity of the atomic interactions increases with increasing temperature, the phonon transmission coefficient is enhanced through inelastic scattering and reduces the ITR [27,44,45]. A similar trend has been reported for the ITR at some other inter-

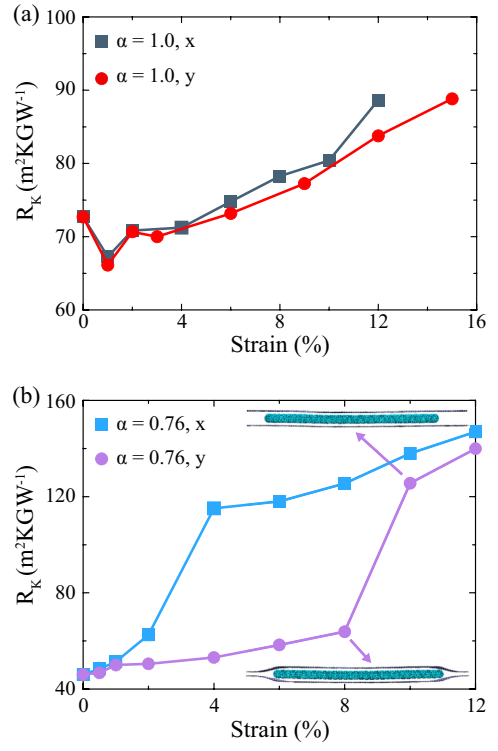

Fig. 6. Effect of the in-plane strain on the ITR. (a) The dependence of the ITR on the in-plane tensile strain with $\alpha = 1.0$. (b) The dependence of the ITR on the in-plane tensile strain with $\alpha = 0.76$. Insets are the structures under the strain of 8% and 10%..

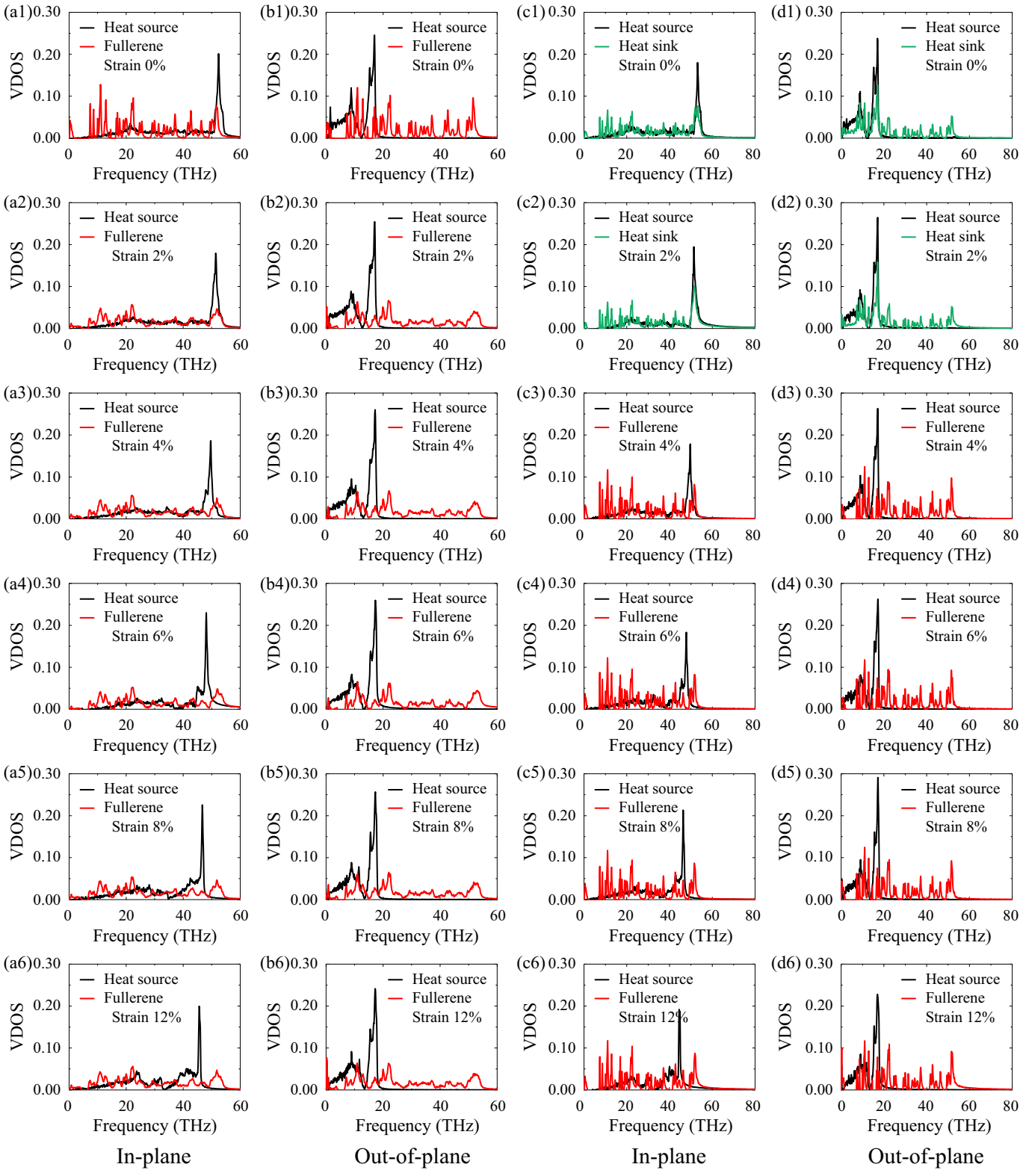

Fig. 7. Phonon VDOS. (a1)-(a6) The in-plane phonon VDOS for the GFG with $\alpha = 1.0$. (b1)-(b6) The out-of-plane phonon VDOS for the GFG with $\alpha = 1.0$. (c1)-(c6) The in-plane phonon VDOS for the GFG with $\alpha = 0.76$. (d1)-(d6) The out-of-plane phonon VDOS for GFG with $\alpha = 0.76$. The strain is applied along the x direction.

faces, such as the graphene/black phosphorus interface [27], Si/Ge interface [44].

For the GFG structure with $\alpha = 0.76$, there is a jump for the ITR at 600 K, at which the value of the ITR is enhanced by about a factor of two. We thus also observe that the on/off switchable ITR can be manipulated by the temperature. The origin of this jump is also due to the transition from the adhered configuration below 600 K to the separated configuration above 600 K as illustrated by the insets in Fig. 5. A similar jump phenomenon can also be observed in the GFG structures with the area ratio $\alpha = 0.81$.

3.3. Strain effect

3.3.1. In-plane tensile strain effect

We investigate the effect of tensile strain on the ITR of the GFG heterostructure with $\alpha = 1.0$ and 0.76, which are greater and less than the α_{c2}, respectively. The ITR at room temperature in GFG sandwich structures under uniaxial tensile strain in x and y directions is shown in Fig. 6. As shown in Fig. 6(a), there is no structure transition for the GFG sandwich ($\alpha = 1.0$) with increasing strain, and as such the ITR can be slightly enhanced with increasing strain. However, the on/off switchable thermal resistance also emerges in Fig. 6(b) for the GFG structure with $\alpha = 0.76$, where the ITR is enhanced by about a factor of two. Unlike the increasing temperature case in Fig. 5, the ITR continues to increase after the jump with increasing strain, and the point of the following analysis will be to explain why that happens. The transition from the adhered configuration below 8% strain to the separated configuration above 10% strain is illustrated by the insets in Fig. 6(b).

To further assess the impact of the in-plane stretching strain, two mechanisms are mainly considered. One is the contact area effect, which is shown by the analytic expression Eq. (8). It can well describe the size dependence for the ITR jump as shown in the Fig. 4(b). The other mechanism is the overlap of the phonon vibrational density of states (VDOS). The vibration power spectrum can capture the effect of atomic vibrations on the interfacial thermal transport. This quantity has been used to understand the thermal transport for graphene/phosphorene [26], silicene/graphene [46], and graphene/black phosphorus [27] interfaces. The phonon VDOS $P(\omega)$ at the frequency ω which can be calculated by performing the Fourier transform on the velocity auto-correlation function as [47]

$$P(\omega) = \frac{1}{\sqrt{2\pi}} \int_0^\infty e^{i\omega t} < \sum_{j=1}^{N} v_j(t) v_j(0) > d\omega, \tag{9}$$

where $v_j(t)$ denotes the velocity of the atom j at time t. To quantify the match between the vibration spectra of atoms at the interfaces, an overlap factor S is defined based on the correlation parameter, which is employed to explore the insight of interfacial interactions [48]

$$S = \frac{\int_0^\infty P_{Heat}(\omega) P_{cold}(\omega) d\omega}{\int_0^\infty P_{Heat}(\omega) d\omega \int_0^\infty P_{cold}(\omega) d\omega}, \tag{10}$$

where $P_{Heat}(\omega)$ and $P_{Cold}(\omega)$ denotes the phonon spectra at frequency ω of heat source and heat sink at the interface, respectively.

The GFG heterostructure with the area ratio $\alpha = 1.0$ exhibits no structural changes under the in-plane tensile strain. Thus, the strain dependence for the ITR is mainly due to the effect of the VDOS overlap. The in-plane VDOS and the out-of-plane VDOS of graphene and fullerene under various strains in the x direction are shown in the Figs. 7(a) and (b), respectively. For the in-plane VDOS, the peak of the graphene phonon shifts to low frequencies, while the peak of the fullerene phonon is almost unchanged. As shown in Fig. 8(a), the corresponding overlap decreases as the in-plane tensile strain increases, which illustrates that the phonon coupling strength is reduced. For the out-of-plane VDOS, the peak of the graphene phonon slightly shifts to high frequencies, while the peak of the fullerene phonon is almost unchanged. The corresponding overlap increases as the in-plane tensile strain increases, as shown in Fig. 8(a). This illustrates that the phonon coupling strength is enhanced. Even if the overlap of in-plane and out-of-plane VDOS has an opposite trend, the increasing ITR of GFG sandwiches with increasing tensile strain is primarily contributed by the in-plane phonons, because the overlap of the in-plane VDOS is larger than that of the out-of-plane VDOS.

For the GFG heterostructure with the area ratio $\alpha = 0.76$, there is a structural transition under the in-plane strain. Thus, the contact area mechanism becomes dominant for the strain dependence of the ITR. Fig. 6(b) shows that the ITR has a jump when the strain is large enough to drive the structure to transit from the adhered configuration to the separated configuration. This is a direct result of the reduction of the contact area after the structural transition. The structural transition can also affect the overlap of VDOS. The overlaps of in-plane and out-of-plane VDOS are shown in Fig. 8(b), which has a step-like change at the structural transition (the 2% – 4% strain in x direction and the 8% – 10% strain in y direction). Therefore, the jump of ITR with increasing tensile strain is primarily due to the contact area effect, and the VDOS overlap also plays an important role. The GFG heterostructure is more sensitive to the in-plane tensile strain along the x direction, so we have shown the variation of VDOS with the tensile strain in the x direction.

Figs. 5 and 6 also show that the temperature range over which the jump in ITR occurs can be enlarged using uniaxial mechanical strain. This is in contrast to phase transition methods for which the materials work only in fixed temperature ranges [5]. For example, while no transition in the ITR is observed in Fig. 5 for $\alpha = 0.76$ at 300 K, the jump transition can be induced at the room temperature for $\alpha = 0.76$ using uniaxial strain as shown in Fig. 6. Thus the GFG sandwich structure can adopt different structures instead of needs of the environment.

3.3.2. Cross-plane compressive strain effect

We finally investigate the effect of cross-plane compressive strain on the ITR of the GFG heterostructure. The dimension of the

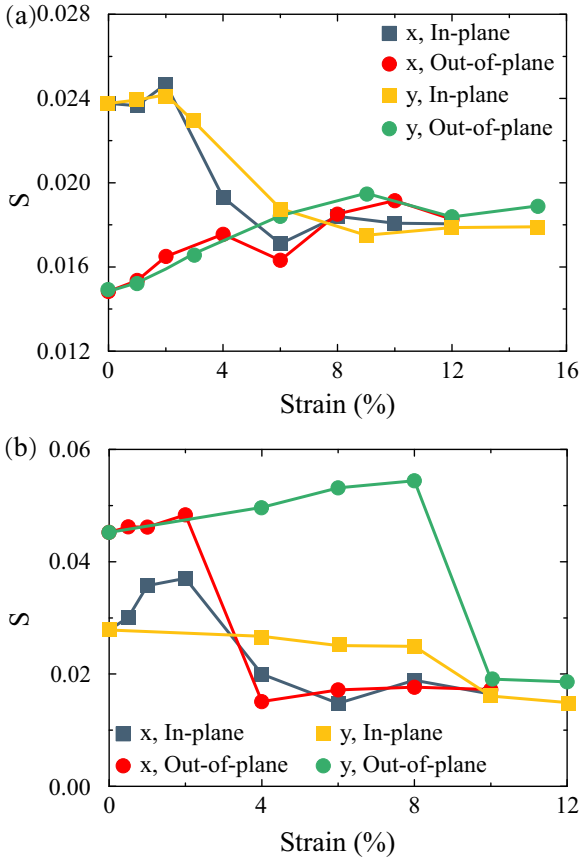

Fig. 8. Overlap S of phonon VDOS as a function of the in-plane stretch strain for the GFG with (a) $\alpha = 1.0$ and (b) $\alpha = 0.76$..

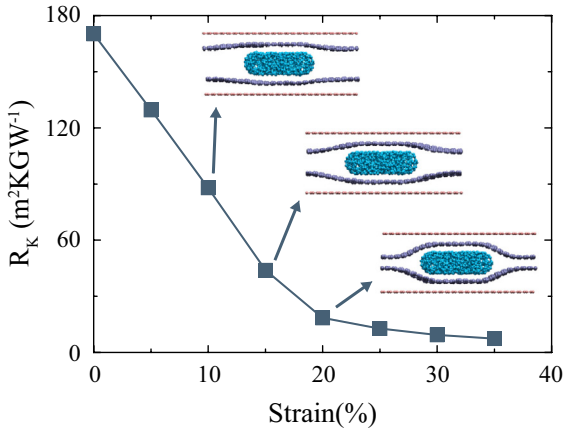

Fig. 9. The cross-plane compressive strain effect on the ITR. Insets display the atomic configuration for the GFG interface at the strain of 10%, 15% and 20%..

GFG heterostructure is 5.04×5.09 nm^2, and the area ratio α is 0.4, which is greater than the α_{c2}. As shown in Fig. 9, the ITR decreases monotonically with the increase of the cross-plane compressive strain. It is similar to several other Van der Waals heterostructures, such as graphene/MoS_2 heterostructures [31], graphene/black phosphorus heterostructures [27], and porous carbon foams [49]. The decrease of ITR induced by compressive strain is due to two main reasons. First, the compression on the Van der Waals heterostructures reduces the interlayer distance, and therefore increases the strength of the interlayer interaction. Second, the phonon coupling strength is enhanced. The cross-plane compressive strain enhances the interfacial stiffness and results in the stiffening of the phonons transferring across interlayers, which leads to an increase in the phonon group velocity and the average phonon transmission coefficient [27,49].

The jump in the insets in Fig. 9 demonstrates that the structure changes at the cross-plane compressive strain of 20%. As shown in Fig. 9, the ITR decreases gradually during the structure transition from the separated configuration to the adhered configuration for the GFG heterostructure. This is because the GFG sandwich structure has a better thermal transport ability under large cross-plane compressive strain. Then the contribution of structural changes to ITR is not significant, even if graphene layers are adsorbed together to increase the Van der Waals interaction.

4. Conclusion

In summary, we have proposed nanoscale sandwich-like heterostructures to serve as thermal switches. The GFG sandwich is used as an example to study the thermal hysteresis by the heat dissipation MD simulations. We find that the ITR shows a step-like enhancement at a critical point by varying the number of fullerene, where the magnitude of the ITR can be enhanced by a factor of two. The origin of this switchable behavior is the structure transition of the GFG sandwich from the adhered configuration to the separated configuration of the outer two graphene layers. These simulation results are explained by analytic expressions based on the heat transport theory. We further show that the temperature and strain can efficiently manipulate the step-like phenomenon. Finally, we demonstrated that in contrast to phase change methods of heat transfer, while the step-like enhancements of the ITR can be induced at certain temperatures, the temperature range can be increased using uniaxial mechanical strain. This work thus demonstrates that sandwich-like nanoscale heterostructures can exhibit hysteretic changes in heat transport, and thus show promise for potential applications in switchable thermal devices.

Declaration of Competing Interest

The authors declare that they have no known competing financial interests or personal relationships that could have appeared to influence the work reported in this paper.

CRediT authorship contribution statement

Yixuan Xue: Conceptualization, Data curation, Writing – original draft. **Harold S. Park:** Conceptualization, Writing – review & editing. **Jin-Wu Jiang:** Conceptualization, Writing – review & editing, Funding acquisition.

Data availability

Data will be made available on request.

Acknowledgment

This work is supported by the National Natural Science Foundation of China (Grant Nos. 11,822,206 and 12072182), the Innovation Program of the Shanghai Municipal Education Commission (Grant No. 2017-01-07-00-09-E00019), and the Key Research Project of Zhejiang Laboratory (Grant No. 2021PE0AC02).

References

[1] R. Shrestha, Y. Luan, S. Shin, T. Zhang, X. Luo, J.S. Lundh, W. Gong, M.R. Bockstaller, S. Choi, T. Luo, et al., High-contrast and reversible polymer thermal regulator by structural phase transition, Sci. Adv. 5 (12) (2019) eaax3777.
[2] X. Cartoixà, L. Colombo, R. Rurali, Thermal rectification by design in telescopic si nanowires, Nano Lett. 15 (12) (2015) 8255–8259.
[3] L. Wang, B. Li, Thermal memory: a storage of phononic information, Phys. Rev. Lett. 101 (26) (2008) 267203.
[4] G. Wehmeyer, T. Yabuki, C. Monachon, J. Wu, C. Dames, Thermal diodes, regulators, and switches: physical mechanisms and potential applications, Appl. Phys. Rev. 4 (4) (2017) 041304.
[5] K. Kim, M. Kaviany, Thermal conductivity switch: optimal semiconductor/metal melting transition, Phys. Rev. B 94 (15) (2016) 155203.
[6] R. Zheng, J. Gao, J. Wang, G. Chen, Reversible temperature regulation of electrical and thermal conductivity using liquid–solid phase transitions, Nat. Commun. 2 (1) (2011) 1–6.
[7] J. Cho, M.D. Losego, H.G. Zhang, H. Kim, J. Zuo, I. Petrov, D.G. Cahill, P.V. Braun, Electrochemically tunable thermal conductivity of lithium cobalt oxide, Nat. Commun. 5 (1) (2014) 1–6.
[8] J. Kimling, R.B. Wilson, K. Rott, J. Kimling, G. Reiss, D.G. Cahill, Spin-dependent thermal transport perpendicular to the planes of co/cu multilayers, Phys. Rev. B 91 (14) (2015) 144405.
[9] I. Seshadri, A. Gardner, R.J. Mehta, R. Swartwout, P. Keblinski, T. Borca-Tasciuc, G. Ramanath, Gating heat transport by manipulating convection in a magnetic nanofluid, Appl. Phys. Lett. 102 (20) (2013) 203111.
[10] W. Yu, H. Xie, L. Yin, J. Zhao, L. Xia, L. Chen, Exceptionally high thermal conductivity of thermal grease: synergistic effects of graphene and alumina, Int. J. Therm. Sci. 91 (2015) 76–82.
[11] J. Yang, Y. Yang, S.W. Waltermire, X. Wu, H. Zhang, T. Gutu, Y. Jiang, Y. Chen, A.A. Zinn, R. Prasher, et al., Enhanced and switchable nanoscale thermal conduction due to van der waals interfaces, Nat. Nanotechnol. 7 (2) (2012) 91–95.
[12] C.-W. Chang, D. Okawa, H. Garcia, T.D. Yuzvinsky, A. Majumdar, A. Zettl, Tunable thermal links, Appl. Phys. Lett. 90 (19) (2007) 193114.
[13] W. Yuan, Z. Deng, Z. Ren, Y. Shen, W. Xi, J. Luo, Monolayer goldene intercalated in graphene layers, Appl. Phys. Lett. 117 (23) (2020) 233102.
[14] H. Wang, J. Dong, Y. Yao, Q. Zhang, J. Cheng, H. Yang, Z. Xia, Y. Zhang, X. Qin, Flexible substrate based on sandwich-structure hydrocarbon resin/aligned boron nitride composites with high thermal conductivity and low dielectric loss, Compos. Sci. Technol. 228 (2022) 109654.
[15] C. Yan, T. Yu, C. Ji, D.J. Kang, N. Wang, R. Sun, C.-P. Wong, Tailoring highly thermal conductive properties of te/mos2/ag heterostructure nanocomposites using a bottom-up approach, Adv. Electron. Mater. 5 (1) (2019) 1800548.
[16] R. Mirzayev, K. Mustonen, M.R.A. Monazam, A. Mittelberger, T.J. Pennycook, C. Mangler, T. Susi, J. Kotakoski, J.C. Meyer, Buckyball sandwiches, Sci. Adv. 3 (6) (2017) e1700176.
[17] D. Olaya, C.-C. Tseng, W.-H. Chang, W.-P. Hsieh, L.-J. Li, Z.-Y. Juang, Y. Hernández, Cross-plane thermoelectric figure of merit in graphene-c60 heterostructures at room temperature, Flat Chem. 14 (2019) 100089.
[18] T. Verhagen, V. Vales, M. Kalbac, J. Vejpravova, Temperature-induced evolution of strain and doping in an isotopically labeled two-dimensional graphene-c70 fullerene peapod, Diam. Relat. Mater. 75 (2017) 140–145.
[19] Y. Xue, J.-W. Jiang, H.S. Park, A universal law for the pattern evolution of fullerene-based sandwiches, arXiv preprint arXiv:2211.09725 (2022).

[20] S. Plimpton, Fast parallel algorithms for short-range molecular dynamics, J. Comput. Phys. 117 (1) (1995) 1–19.
[21] W. Humphrey, A. Dalke, K. Schulten, Vmd: visual molecular dynamics, J. Mol. Graph. 14 (1) (1996) 33–38.
[22] Y. Zhao, Y. Song, Z. Hu, W. Wang, Z. Chang, Y. Zhang, Q. Lu, H. Wu, J. Liao, W. Zou, et al., Large-area transfer of two-dimensional materials free of cracks, contamination and wrinkles via controllable conformal contact, Nat. Commun. 13 (1) (2022) 4409.
[23] Z. Li, Y. Wang, M. Ma, H. Ma, W. Hu, X. Zhang, Z. Zhuge, S. Zhang, K. Luo, Y. Gao, et al., Ultrastrong conductive in situ composite composed of nanodiamond incoherently embedded in disordered multilayer graphene, Nat. Mater. 22 (1) (2023) 42–49.
[24] L. Verlet, Computer "experiments" on classical fluids. i. thermodynamical properties of lennard-jones molecules, Phys. Rev. 159 (1) (1967) 98–103.
[25] R.J. Stoner, H.J. Maris, Kapitza conductance and heat flow between solids at temperatures from 50 to 300 k, Phys. Rev. B: Condens. Matter 48 (22) (1993) 16373.
[26] Y. Hong, J. Zhang, X.C. Zeng, Interlayer thermal conductance within a phosphorene and graphene bilayer, Nanoscale 8 (46) (2016) 19211–19218.
[27] Y. Chen, Y. Zhang, K. Cai, J. Jiang, J.C. Zheng, J. Zhao, N. Wei, Interfacial thermal conductance in graphene/black phosphorus heterogeneous structures, Carbon N Y 117 (2017) 399–410.
[28] H.J.C. Berendsen, J.v. Postma, W.F. van Gunsteren, A. DiNola, J.R. Haak, Molecular dynamics with coupling to an external bath, J. Chem. Phys. 81 (8) (1984) 3684–3690.
[29] Z. Xu, M.J. Buehler, Heat dissipation at a graphene–substrate interface, J. Phys.: Condens. Matter 24 (47) (2012) 475305.
[30] Y. Xue, J.-W. Jiang, Strain engineering for the kapitza resistance of the zro2/alpha-al2o3 and YSZ/alpha-al2o3 interfaces, Acta Mech. Solida Sin. 35 (1) (2022) 101–112.
[31] Z. Ding, Q.-X. Pei, J.-W. Jiang, W. Huang, Y.-W. Zhang, Interfacial thermal conductance in graphene/mos2 heterostructures, Carbon N Y 96 (2016) 888–896.
[32] X. Liu, G. Zhang, Y.-W. Zhang, Topological defects at the graphene/h-BN interface abnormally enhance its thermal conductance, Nano Lett. 16 (8) (2016) 4954–4959.
[33] Y. Wang, Z. Qin, M.J. Buehler, Z. Xu, Intercalated water layers promote thermal dissipation at bio–nano interfaces, Nat. Commun. 7 (1) (2016) 1–7.
[34] D. Alexeev, J. Chen, J.H. Walther, K.P. Giapis, P. Angelikopoulos, P. Koumoutsakos, Kapitza resistance between few-layer graphene and water: liquid layering effects, Nano Lett. 15 (9) (2015) 5744–5749.
[35] J. Chen, J.H. Walther, P. Koumoutsakos, Strain engineering of kapitza resistance in few-layer graphene, Nano Lett. 14 (2) (2014) 819–825.
[36] A. Morozenko, I.V. Leontyev, A.A. Stuchebrukhov, Dipole moment and binding energy of water in proteins from crystallographic analysis, J. Chem. Theory Comput. 10 (10) (2014) 4618–4623.
[37] P.P. Romańczyk, M. Radoń, K. Noga, S.S. Kurek, Autocatalytic cathodic dehalogenation triggered by dissociative electron transfer through a c–h–o hydrogen bond, PCCP 15 (40) (2013) 17522–17536.
[38] S. Lin, M.J. Buehler, The effect of non-covalent functionalization on the thermal conductance of graphene/organic interfaces, Nanotechnology 24 (16) (2013) 165702.
[39] A. Bagri, S.-P. Kim, R.S. Ruoff, V.B. Shenoy, Thermal transport across twin grain boundaries in polycrystalline graphene from nonequilibrium molecular dynamics simulations, Nano Lett. 11 (9) (2011) 3917–3921.
[40] L. Hu, T. Desai, P. Keblinski, Determination of interfacial thermal resistance at the nanoscale, Phys. Rev. B 83 (19) (2011) 195423.
[41] M.A. Angadi, T. Watanabe, A. Bodapati, X. Xiao, O. Auciello, J.A. Carlisle, J.A. Eastman, P. Keblinski, P.K. Schelling, S.R. Phillpot, Thermal transport and grain boundary conductance in ultrananocrystalline diamond thin films, J. Appl. Phys. 99 (11) (2006) 114301.
[42] P.K. Schelling, S.R. Phillpot, P. Keblinski, Kapitza conductance and phonon scattering at grain boundaries by simulation, J. Appl. Phys. 95 (11) (2004) 6082–6091.
[43] J.L. Rivera, C. McCabe, P.T. Cummings, Molecular simulations of liquid-liquid interfacial properties: water–n-alkane and water–methanol–n-alkane systems, Phys. Rev. E 67 (1) (2003) 011603.
[44] T. Zhan, S. Minamoto, Y. Xu, Y. Tanaka, Y. Kagawa, Thermal boundary resistance at si/ge interfaces by molecular dynamics simulation, AIP Adv. 5 (4) (2015) 047102.
[45] Z. Wei, Z. Ni, K. Bi, M. Chen, Y. Chen, Interfacial thermal resistance in multilayer graphene structures, Phys. Lett. A 375 (8) (2011) 1195–1199.
[46] B. Liu, J.A. Baimova, C.D. Reddy, A.W.-K. Law, S.V. Dmitriev, H. Wu, K. Zhou, Interfacial thermal conductance of a silicene/graphene bilayer heterostructure and the effect of hydrogenation, ACS Appl. Mater. Interfac. 6 (20) (2014) 18180–18188.
[47] B.R. Mollow, Power spectrum of light scattered by two-level systems, Phys. Rev. 188 (5) (1969) 1969–1975.
[48] J. Lan, B. Li, Thermal rectifying effect in two-dimensional anharmonic lattices, Phys. Rev. B 74 (21) (2006) 214305.
[49] X.-K. Chen, X.-Y. Hu, P. Jia, Z.-X. Xie, J. Liu, Tunable anisotropic thermal transport in porous carbon foams: the role of phonon coupling, Int. J. Mech. Sci. 206 (2021) 106576.